

Schlieren visualisation and measurement of axisymmetric disturbances

B. R. Sutherland, M. R. Flynn, and K. Onu

Dept. of Mathematical and Statistical Sciences, University of Alberta, Edmonton, Alberta, Canada

Received: 8 July 2002 – Revised: 13 August 2002 – Accepted: 16 August 2002

Abstract. Synthetic schlieren is a new technique that allows one easily and inexpensively to visualise density variations, such as those caused by internal waves propagating in a density stratified fluid. In the special case of two-dimensional internal waves (for example, those created by an oscillating cylinder), synthetic schlieren allows one to measure non-intrusively the wave amplitudes everywhere in space and time. The technique works by measuring the apparent displacement of points in a digitised image (such as a grid of horizontal lines), which is observed by a CCD camera through the experimental test section. Synthetic schlieren is sufficiently sensitive that it can measure sub-pixel-scale disturbances.

In this work, we report on the first step toward measuring fully three-dimensional disturbances. We perform laboratory experiments in which internal waves are generated in a uniformly salt-stratified fluid by a vertically oscillating sphere. Theory predicts that the resulting wave-field is in the form of two cones emanating above and below the sphere. Using inverse tomographic techniques, we exploit the axisymmetry of the wave-field to relate the apparent displacement of pixels in an image to the wave amplitudes.

1 Introduction

Schlieren methods have often been employed to visualise density changes due to internal waves in salt-stratified fluid (Mowbray, 1967; Stevenson, 1969). Density changes are visualised by making use of the way light is bent as it passes through a medium with varying salinity and, hence, varying index of refraction. Traditional schlieren systems, which require two parabolic mirrors (or a pair of masks in the Moiré method (Sakai, 1990; Dalziel et al., 2000)), are limited by several factors including the size of the region being examined (typically less than 1 m), the necessarily accurate posi-

tioning of the mirrors, and the sensitivity to optical imperfections on the mirror surface and test section of the experiment. Furthermore, because mirrors are prone to damage traditional schlieren is prohibitively difficult to employ outside controlled laboratory conditions. In contrast, “synthetic schlieren” is much less expensive and easier to implement: the field of view can be as large as required to visualise the density fluctuations and the positioning does not need to be precise. In addition, digital enhancement provides greater sensitivity and the ability in some geometries to measure the amplitude of internal waves.

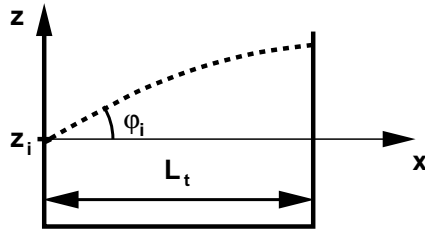
The typical setup to visualise density changes using synthetic schlieren is shown in Fig. 1. We place an “object-image” on the opposite side of the test-section of a tank from a CCD or video camera. In this work, the object-image is composed of equally spaced horizontal black and white lines. The camera is hooked up to a computer so that synthetic schlieren (which reveals the spatial structure of disturbances) is used in real-time, and at later times recorded images are processed to compute the amplitudes of disturbances.

Synthetic schlieren works by comparing an object-image during an experiment with a snap shot taken at an earlier time. This is done by subtracting the intensities of one image by the other on a pixel-by-pixel basis. If there is no change, subtracting the digitised images produces a uniform (e.g. black) schlieren image. If, for example, heat fluctuations cause the real-time object-image to differ from the initial object-image, then subtracting the two images will reveal where the differences occur, and so show the spatial extent of the fluctuations. The difference can be multiplied by an arbitrary constant to further enhance the fluctuations.

This is the use of synthetic schlieren in “qualitative mode”. In special circumstances, synthetic schlieren can be also be used in “quantitative mode”, meaning that the strength of the fluctuations can themselves be measured.

Until recently the quantitative mode could be applied only for fluctuations that were uniform along the line-of-sight of the camera, as in the case of internal waves generated by an oscillating cylinder (Sutherland et al., 1999; Sutherland

a) Side view of test section



b) Light ray path from object-image to camera

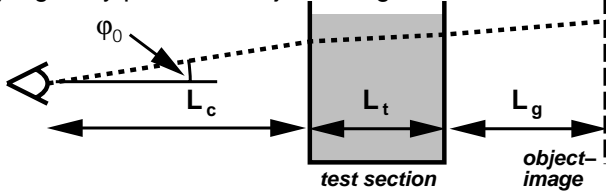


Fig. 1. Path of light ray (a) through tank and (b) from object image to camera.

and Linden, 2002) or flow over a spanwise-uniform barrier (Sutherland and Linden, 1998).

Here we describe how the quantitative mode can be used to measure the amplitude of axisymmetric internal waves, such as those generated by an oscillating sphere. This work complements the results of two other papers that first discussed measuring axisymmetric internal waves using synthetic schlieren. Onu et al. (2002) describes in detail the derivation of equations for a light ray passing through a stratified medium and also describes the inversion process used to measure wave amplitudes from recorded deflections of light rays. Flynn et al. (2002) compares the results of synthetic schlieren with the theoretical prediction for the amplitude of waves generated by an oscillating sphere. Here we illustrate the range of analyses that can be performed using synthetic schlieren to measure axisymmetric disturbances, using the case of waves generated by an oscillating sphere as an example. In particular, we describe in detail how displacements of the object image are calculated and we compare analyses of the change in the squared buoyancy frequency with its time derivative.

Section 2 describes how the internal wave amplitudes are measured using synthetic schlieren. Section 3 presents some experimental results and conclusions are given in Sect. 4.

2 Schlieren method

The process of measuring axisymmetric wave amplitudes involves three steps: digitizing the object image as it is distorted by density fluctuations, computing apparent displacements of components of the image and from these computing wave amplitudes. Each step is described below.

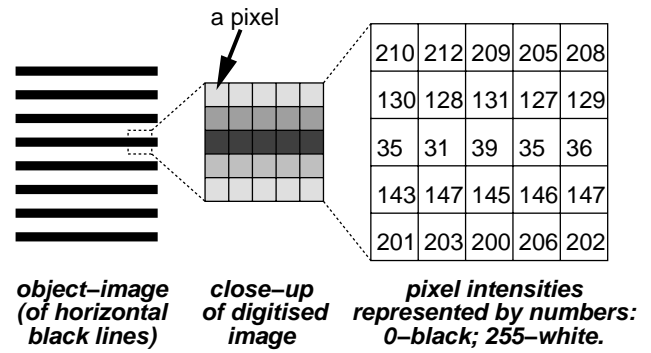


Fig. 2. Close-up of pixels and their corresponding intensities.

2.1 Digitization

Digitisation is done by a DCR-VX1000 Sony camera which continually passes signals of the object image to a Data Translation (DT2861) 16 buffer frame-grabber card.

Figure 2 schematically illustrates the process of digitisation. In the example, it is supposed that the camera records a grey-scale picture of an object-image of horizontal black lines. (The object-image can be colour, but the computer makes practical use only of the intensity information). The digitised image subdivides the object-image into a regular grid of pixels. The incident light is averaged over the area of the pixel so that, for example, a pixel centred on the edge of a black line, will be gray – the average of the black and white regions which each span half the pixel area. If a larger area of the black line spans the pixel then the pixel will be a darker shade of gray.

The effective area of the pixel depends upon the area of the field of view and the pixel resolution. Optimally, the vertical distance between adjacent black lines should be spanned by 5 to 6 pixels. This can be used as a guide to the thickness of lines in the object-image. For example, suppose the camera is focussed on a 1 metre square area of the object-image and suppose the digitised image has a resolution of 512 by 512 pixels, the resolution of the DT2861 frame-grabber card. Then, for optimal use of synthetic schlieren, the horizontal lines on the object-image should be spaced vertically apart by a distance of approximately $5 \times \frac{1\text{m}}{512} \simeq 1\text{ cm}$. Each line should be approximately 0.2 cm thick.

In the digitised image, each pixel is assigned an 8-bit integer (0 – 255), representing the average intensity of light over the pixel. A black pixel has value zero, a white pixel has value 255, and gray values lie in between. Thus a digitised image may be stored on a computer as a 512×512 matrix of integers.

2.2 Computing apparent line displacements

To compute the apparent displacement of horizontal black lines in the object image, the digital camera first takes a snapshot of a mesh of horizontal and vertical lines with known spacing. Typically a “world co-ordinate map” is determined

by using this snapshot to identify the position of four pixels near the corners of the mesh image. By interpolation, the position of the remaining pixels is then determined. Keeping the camera stationary, the same world co-ordinate map is used to determine the position of the pixels in the object-image of horizontal lines.

During the course of an experiment, the lines in the object-image appear to move vertically up and down due to light rays passing through regions of spatio-temporally varying density in the test-section of the tank. The displacement can be measured provided it is small compared with the spacing between adjacent horizontal lines. To illustrate the computation, we consider the pixel with intensity $I_0 = 131$ situated above the centre pixel in the right-most schematic in Fig. 2. The intensity of the pixels above and below are $I_1 = 209$ and $I_{-1} = 39$, respectively. When the black line appears to be displaced upward the middle pixel will decrease in intensity, for example to a value of $I_0' = 101$.

We perform a quadratic interpolation to estimate the resulting apparent vertical displacement of the line. In the above example, we suppose the upper, middle and lower pixels are situated at relative vertical positions $z_1 = 0.05$ cm, $z_0 = 0$ cm and $z_{-1} = -0.05$ cm, respectively. Then the vertical displacement of the middle line is given by

$$\Delta z = (z_{-1} - z_0) \frac{(I_0' - I_0)(I_0' - I_1)}{(I_{-1} - I_0)(I_{-1} - I_1)} + (z_1 - z_0) \frac{(I_0' - I_0)(I_0' - I_{-1})}{(I_1 - I_0)(I_1 - I_{-1})}. \quad (1)$$

Equation (1) is used to determine apparent vertical displacement only if two conditions are satisfied. First, the pixel must correspond to the “edge” of a line as characterised by the following conditions: $I_{-1} < I_0 < I_1$ (on the upper-edge of a black line) or $I_{-1} > I_0 > I_1$ (on the lower-edge of a black line). Second, in order to reduce sensitivity to signal noise, the intensity differences must exceed a threshold: $|I_{-1} - I_0| > I_{\min}$ and $|I_1 - I_0| > I_{\min}$. Typically, we set $I_{\min} = 10$.

For pixel intensities that do not meet these two conditions, the quadratic interpolation is not performed in this first pass. Their values are instead determined in the second pass by finding the weighted average of the surrounding values of Δz that were found in the first pass. We use a Gaussian weighted average with largest weight given to pixels within $\sigma = 2$ pixels of the centre pixel.

The result of this calculation is a matrix of data $\Delta z(y, z)$, where y and z are the along-tank and vertical co-ordinates, respectively. An example is shown in Fig. 3.

2.3 Computing wave amplitudes from image distortion

The relationship between Δz and the amplitude of disturbances in the tank is found by using Snell’s Law to determine an equation for $z(x)$, the vertical position of the path of a light beam as it passes in the x -direction across the tank. (Because the object-image is composed of horizontal lines, with negligible horizontal variation, we ignore deflections in

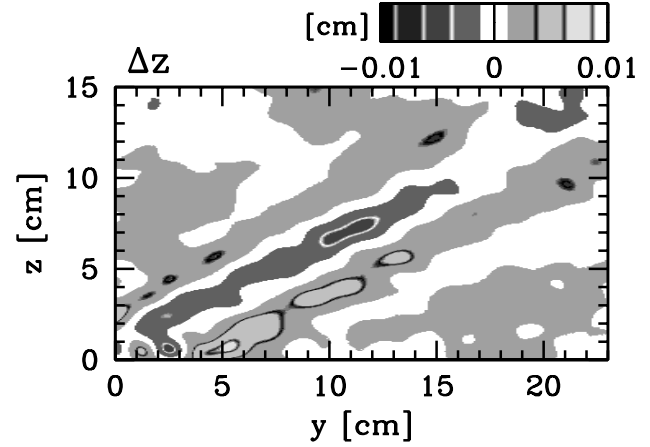


Fig. 3. Vertical pixel displacement, Δz , measured in an oscillating sphere experiment.

the y -direction.) Assuming the light ray is close to the horizontal, we find that $z(x)$ satisfies the nonlinear differential equation (Onu et al., 2002)

$$z'' \left(z' \frac{1}{\frac{\partial n}{\partial x}} + \frac{1}{\frac{\partial n}{\partial z}} \right) = \frac{1}{n} \quad (2)$$

where $n(x, z)$ is the refractive index of salt water. Its value is related to the density, ρ by $n = n_{00} + (\Delta n / \Delta \rho)(\rho - \rho_{00})$ in which $n_{00} \simeq 1.3330$ and $\rho_{00} \simeq 0.99823$ g/cm³ are the index of refraction and density of fresh water at room temperature, respectively. $\Delta n / \Delta \rho \simeq 0.2457$ cm³/g is the rate of change of the index of refraction with salt water density.

Equation (2) is further simplified by assuming the rise in the path of the light ray across the tank is so small that locally n varies approximately linearly with z , so that

$$n(x, z) \simeq n_0(x) - \gamma n_{00} N^2(x) z, \quad (3)$$

where N^2 is the squared buoyancy frequency. This is proportional to the vertical gradient in the index of refraction by a constant factor $-\gamma n_{00}$, in which

$$\gamma = \frac{1}{g} \frac{\rho_{00}}{n_{00}} \frac{\Delta n}{\Delta \rho} \simeq 1.878 \times 10^{-4} \text{ s}^2/\text{cm}.$$

Owing to the small value of γ , perturbation theory allows us to find approximate analytic solutions to Eq. (2).

In particular, if the distortion of isopycnals is uniform across the tank, so that n_0 and N^2 are independent of x , we find (Sutherland and Linden, 1998)

$$z(x) = z_i + x \tan \varphi_i - \frac{1}{2} \gamma N^2 x^2, \quad (4)$$

where z_i is the vertical position and φ_i is the (small) angle to the horizontal at which the light ray enters the tank (see Fig. 1a).

It follows immediately from Eq. (4) that the path of the light ray is bent to a greater degree if the density gradient is

larger and it is bent to a lesser degree if the density gradient is smaller.

For axisymmetric disturbances n_0 and N^2 are, more generally, functions of x . Assuming that the scale, L_x , of horizontal spatial variations in the wave-field is on the order of one to ten times larger than the scale of vertical variations, we find (Onu et al., 2002)

$$z \simeq z_i + x \tan \varphi_i - \gamma n_0 \int_0^x \int_0^{\hat{x}} \frac{N^2(\hat{x})}{n(\hat{x})} d\hat{x} d\hat{x}. \quad (5)$$

This reduces to Eq. (4) in the special case where N^2 and n_0 are x -independent.

Equation (5) gives the path of the light ray as a function of N^2 , which is a combination of its background, N_0^2 , and perturbation, ΔN^2 , value. The change, Δz , in the path of the light ray is given by summing the total rise in the light ray from the camera to object-image and then by subtracting the background contribution. Thus we find

$$\Delta z = -\gamma n_0 \left\{ L_g \frac{n_0}{n_{\text{air}}} \int_0^{L_t} \Delta N^2(x) dx + \int_0^{L_t} \int_0^x \Delta N^2(\hat{x}) d\hat{x} dx \right\}, \quad (6)$$

where $n_{\text{air}} \simeq 1.000$ is the index of refraction of air, L_t is the width of the tank and L_g is the distance from the tank to the image, as illustrated in Fig. 1b. The second term in parentheses represents the deflection of the beam as it passes through the tank; the first term represents the deflection due to the change in angle of the light ray leaving the tank on the side of the object-image.

The problem of finding internal wave amplitudes then reduces to inverting Eq. (6) to find $\Delta N^2(\underline{r})$ given $\Delta z(y, z)$, where generally \underline{r} is vector three-dimensional space. For a general three dimensional disturbance, this problem is ill-posed because the dimensions of \underline{r} and (x, z) differ. However, the problem can be solved exactly if ΔN^2 is an axisymmetric disturbance. That is, if the vector \underline{r} can be represented equivalently by (R, z) , in which R is the radial horizontal distance from the centre of the axisymmetric disturbance.

The inverse problem is solved by representing the integrals in Eq. (6) as matrices acting on the discretely sampled representation of $\Delta N^2(R, z)$, inverting the matrices, and multiplying these by the discrete matrix $\Delta z(y, z)$. The procedure is described in detail by Onu et al. (2002). Typical processing time to determine a single matrix of ΔN^2 values is approximately 10 min. on a 195 MHz R10K CPU of a SGI computer.

3 Results

Here we report on the analysis of experiments performed with a sphere of of radius $a = 1.9$ cm oscillating with frequency $\omega = 0.49 \text{ s}^{-1}$ and half-peak-to-peak amplitude $A = 0.49$ cm. The fluid is uniformly stratified with $N = 0.99 \pm 0.05 \text{ s}^{-1}$. Experiments were performed at least 30 min after filling the tank so that any remnant disturbances evolved

on time-scales much longer than those generated by the oscillating sphere. The sphere is initially at its equilibrium position centred at the origin and then moves periodically vertically downward then upward. Analyses are performed between the second and third period of oscillation, long enough to establish periodic waves in the field of view but not so long that waves have time to reflect from the tank boundaries back into the field of view.

Figure 3 shows the calculated displacement, Δz , of lines in an object image at a time when the sphere has undergone two full oscillations (as it moves downward through its equilibrium position with oscillation phase $\phi = 0^\circ$). Clearly the distortion of the object-image is small: the apparent displacement of lines is less than 0.01 cm. Nonetheless, a coherent pattern along the diagonal from the bottom left to the top right-hand side of the image is evident.

From the $\Delta z(y, z)$ field, one can compute $\Delta N^2(R, z)$. For example, Fig. 4 shows the ΔN^2 field at four different phases of the sphere's oscillation. The images clearly show the downward propagation of lines of constant phase associated with internal waves as time (or, equivalently, the phase of the sphere's oscillation) increases. This is consistent with the prediction of linear theory for internal waves that the group and phase velocity are perpendicular and the sign of their vertical components are opposite to each other.

By finding the root-mean-square (rms) average of the ΔN^2 field computed at successive times during one period of oscillation, we can reconstruct the amplitude envelope of the waves. Assuming the amplitude at each point (R, z) varies sinusoidally as $A_{\Delta N^2} \sin \phi$, then the rms average is $A_{\Delta N^2}/2^{1/2}$. The amplitude envelope is therefore found by multiplying the result at each point by $2^{1/2}$. For example, Fig. 5 shows the amplitude envelope computed by taking the rms average of 16 ΔN^2 fields computed at $\phi = 0^\circ, 22.5^\circ, \dots, 337.5^\circ$, and multiplying the result by $2^{1/2}$.

A detailed analysis of the structure of the wave-beam is performed by taking along and across-beam slices through snapshots of the wave-field, as shown in Fig. 4, and the amplitude envelope, as shown in Fig. 5.

For example, across-beam slices through the ΔN^2 field at two positions along the wave-cone are shown in Fig. 6. The amplitudes are plotted against σ , the across-beam coordinate with positive values on the upper-flank of the wave-beam. At $r/a = 2$, the wave-beam is double peaked, as indicated from the amplitude envelope (heavy solid line). The maximum values occur close to positions where $|\sigma| = a$. The lighter lines show the amplitudes at four instantaneous phases of oscillation. Again, these indicate that the wave crests move downward (to smaller σ) with increasing phase. The asymmetry with respect to σ is due in part to noise and to interference with the downward propagating wave-cone. Farther from the sphere, at $r/a = 10$, the wave-beam envelope exhibits a single peak near $\sigma = 0$. This transition from bimodal to unimodal structure is a result of viscous attenuation and has been examined theoretically in detail by Flynn et al. (2002). At this distance from the sphere, the amplitude

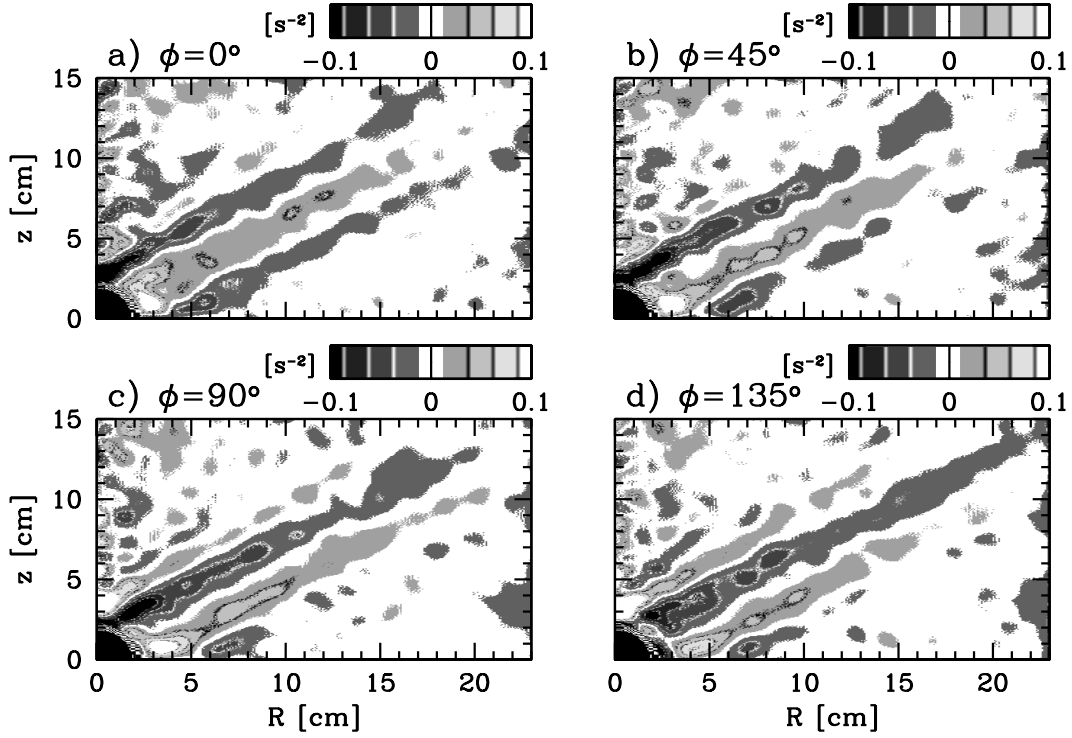


Fig. 4. ΔN^2 field at four different phases of the sphere's oscillation.

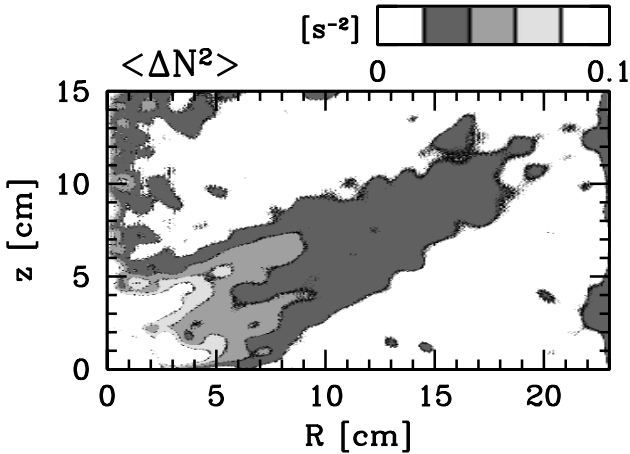


Fig. 5. Amplitude envelope of the ΔN^2 field.

of the waves is approximately one quarter that of the waves at $r/a = 2$, and closer to the noise threshold of 0.01 s^{-2} . The fluctuations due to noise are evident by the discrepancy between the amplitude envelope and instantaneous amplitude of the waves at the four phases shown.

In the discussion above, we have discussed how to compute Δz by comparing the object image during an experiment with the initial image. We can also compare the object image at one time with the image taken a short time Δt earlier. Dividing the resulting Δz field by Δt we determine the approximate time-derivative field Δz_t , which is the speed of

the apparent vertical motion of the lines in the image. An example of fields computed from the time derivative is shown in Fig. 7.

Figure 7a shows the Δz_t field computed by taking the difference between images at phases $\phi = 0^\circ$ and 22.5° . This most accurately represents the pattern of the Δz_t field at the average of the two phases, 11.25° . In comparison with Fig. 3, the field is more contaminated by signal noise. Nonetheless, a coherent upward diagonal pattern resulting from the wave-cone is evident. Furthermore, the pattern reveals a wave-beam that is smaller in amplitude (as measured in cm/s) by approximately half that of the Δz field (as measured in cm), and is advanced in phase.

Likewise, we may compare the N^2_t field, shown in Fig. 7b, with the ΔN^2 field shown in Fig. 4. In particular, we infer that the phase of the N^2_t field most closely matches that of the ΔN^2 field at phase -90° .

These results are consistent with linear theory. For a temporally periodic wave, the time dependence of the wave-field can be represented by a factor $\exp(-i\omega t)$. Thus, we expect the complex representation of the N^2_t and ΔN^2 fields are related by

$$N^2_t \equiv \partial \Delta N^2 / \partial t = -i\omega \Delta N^2. \quad (7)$$

The factor $-i$ gives rise to the -90° phase shift between the fields, and the amplitude difference is accounted for by the factor $\omega \simeq 0.49 \text{ s}^{-1}$.

Finally, we can compare the amplitude envelope of the N^2_t and ΔN^2 fields. As anticipated, both show the transi-

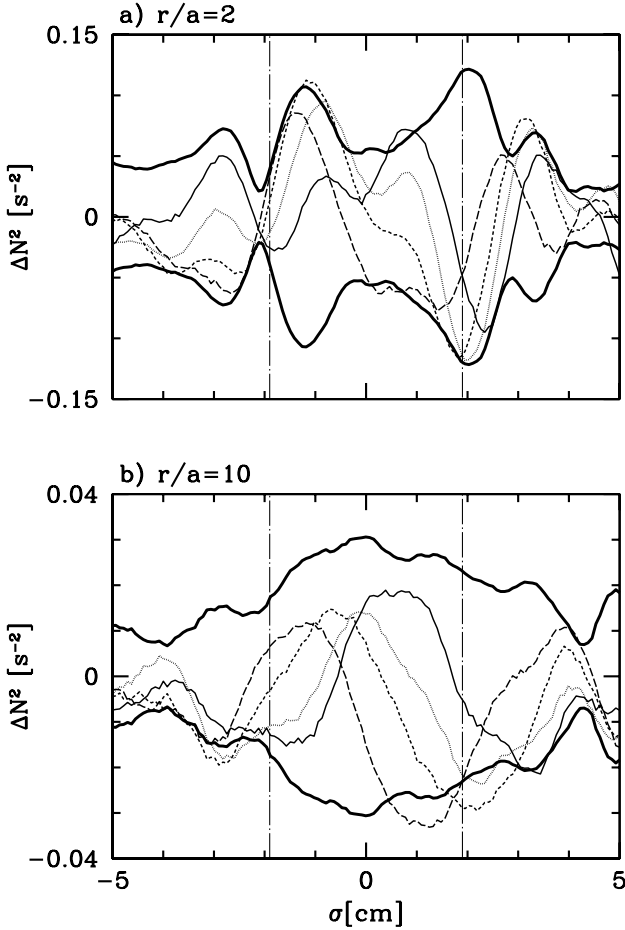


Fig. 6. Measured across-beam amplitude at (a) $r/a = 2$ and (b) $r/a = 10$ of ΔN^2 field at four different phases of oscillation: $\phi = 0^\circ$ (solid line), $\phi = 45^\circ$ (dotted line), $\phi = 90^\circ$ (short-dashed line), $\phi = 135^\circ$ (long-dashed line). The amplitude envelope computed from the $\langle \Delta N^2 \rangle$ field is also shown as the heavy solid lines. The vertical dash-dotted lines indicate the extremities of the sphere.

tion from bimodal to unimodal behaviour with distance from the sphere.

4 Discussion and conclusions

We have described the experimental setup and calculation required to measure axisymmetric internal waves using synthetic schlieren. The techniques give measurements of the change in the buoyancy frequency, $\Delta N^2(R, z)$, and its time derivative, $N^2_t(R, z)$. Although in this application, the ΔN^2 field provides better measurements for these experiments, it is useful to measure N^2_t field in circumstances where the object-image is distorted to such a large degree that a black line shifts by a full line width. In this case, the Δz field cannot be determined because the interpolation given by Eq. (1) is no longer valid. However, if the time difference, Δt , between successive images is sufficiently small, the black line

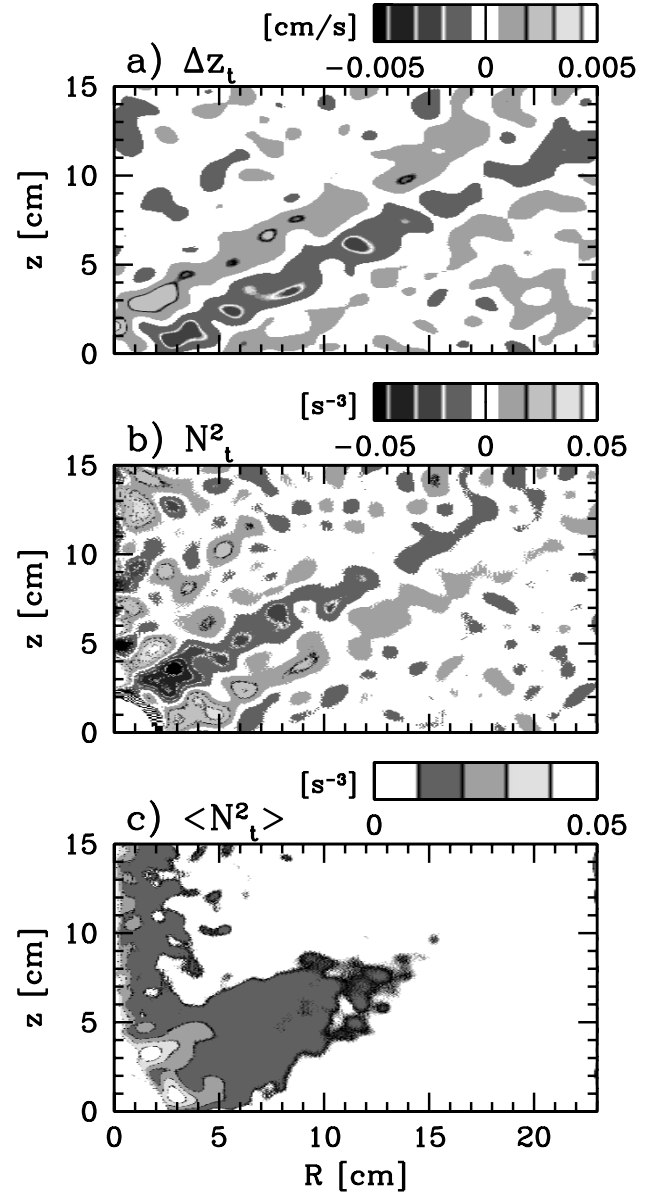


Fig. 7. Measured approximate time derivatives of (a) Δz and (b) ΔN^2 fields at phase 11.25° . The amplitude envelope of the N^2_t field is shown in (c).

will shift by a small amount between the two images and Eq. (1) can be used reliably.

Both ΔN^2 and N^2_t are unusual fields to work with. Assuming wave amplitudes are sufficiently small, however, linear theory may be used to relate these fields to more useful quantities such as the velocity and perturbation density (Sutherland et al., 1999).

Axisymmetric waves and, in particular, internal waves generated by an oscillating sphere have been studied both because this geometry allows one to reconstruct the wave-field from a single camera's perspective and because the experimental results may be compared with the prediction of linear theories (Appley and Crighton, 1987; Voisin, 1991). Indeed,

good agreement is found between the experimental results and a theory that includes the effects of viscous attenuation (Flynn et al., 2002).

Though interesting as an idealized study, the ultimate goal of this research programme is to adapt synthetic schlieren to measure fully three dimensional disturbances. In this case more than one perspective would be required and more sophisticated inverse tomographic techniques employed to reconstruct the wave-field. The success of the present work is encouraging for continued progress in this direction.

References

- Appleby, J. C. and Crighton, D. G.: Internal gravity waves generated by oscillations of a sphere, *J. Fluid Mech.*, 183, 439–450, 1987.
- Dalziel, S. B., Hughes, G. O., and Sutherland, B. R.: Whole field density measurements, *Experiments in Fluids*, 28, 322–335, 2000.
- Flynn, M. R., Onu, K., and Sutherland, B. R.: Internal wave generation by a vertically oscillating sphere, *J. Fluid Mech.*, submitted, 2002.
- Mowbray, D. E.: The use of schlieren and shadowgraph techniques in the study of flow patterns in density stratified liquids, *J. Fluid Mech.*, 27, 595–608, 1967.
- Onu, K., Flynn, M. R., and Sutherland, B. R.: Schlieren measurement of axisymmetric internal wave amplitudes, *Expt. Fluids*, in press, 2002.
- Sakai, S.: Visualisation of internal gravity waves by Moiré method, *Kashika-Joho*, 10, 65–68, 1990.
- Stevenson, T. N.: Axisymmetric internal waves generated by a travelling oscillating body, *J. Fluid Mech.*, 35, 219–224, 1969.
- Sutherland, B. R. and Linden, P. F.: Internal wave generation by flow over a thin barrier, *J. Fluid Mech.*, 377, 223–252, 1998.
- Sutherland, B. R. and Linden, P. F.: Internal wave excitation by a vertically oscillating elliptical cylinder, *Phys. Fluids*, 14, 721–731, 2002.
- Sutherland, B. R., Dalziel, S. B., Hughes, G. O., and Linden, P. F.: Visualisation and measurement of internal waves by “synthetic schlieren”. Part 1: Vertically oscillating cylinder, *J. Fluid Mech.*, 390, 93–126, 1999.
- Voisin, B.: Internal wave generation in uniformly stratified fluids, Part 1, Green’s function and point sources, *J. Fluid Mech.*, 231, 439–480, 1991.